Electronic Supplementary Material (ESI) for Journal of Materials Chemistry B.
This journal is © The Royal Society of Chemistry 2022

Supporting Information

A smart hydrogel patch with high transparency, adhesiveness and hemostasis for all-round treatment and glucose monitoring of diabetic foot ulcers

Hou Liu[a], Zuhao Li[b], Songtian Che[c], Yubin Feng[a], Lin Guan[a], Xinting Yang[a], Yue Zhao*[a], Jincheng Wang*[b], Andrei V. Zvyagin[d], Bai Yang[a] and Quan Lin*[a]

[a]State Key Laboratory of Supramolecular Structure and Materials, College of Chemistry, Jilin University, Changchun, 130012, P. R. China

[b]Orthopaedic Medical Center, The Second Hospital of Jilin University, Changchun 130041, P. R. China

[c]Department of Ocular Fundus Disease, The Second Hospital of Jilin University, Changchun 130022, P. R. China.

[d]Australian Research Council Centre of Excellence for Nanoscale Biophotonics, Macquarie University, Sydney, NSW 2109, Australia and Institute of Biology and Biomedicine, Lobachevsky Nizhny Novgorod State University, 603105. Nizhny Novgorod, Russia

*To whom correspondence should be addressed. E-mail: linquan@jlu.edu.cn; Phone: +86 431-8516-8483; Fax: +86 431-8519-3423

1. Experimental section

1.1 Synthesis of P(Py-TA) nanoparticles

The P(Py-TA) nanoparticles (NPs) were synthesized by a modified polymerization aqueous dispersion method. In brief, 0.7 g PVA was dissolved into 10 mL deionized water at 90 °C with magnetic stirring, until dissolved completely. After the solution was cooled in an ice-water bath, the Py monomer (1 mmol, 70 μL) was added into the PVA solution in a violent rotation. And then, cool $FeCl_3$•$6H_2O$ (2.3 mmol, 0.6 g) and TA (15 mg) were dissolved into the above solution, in turn. The mixed solution was continually stirred in an ice-water bath for 8 h to allow the complete polymerization of the Py and TA monomers. The resulted solution went through centrifugation under 8800 rad/s and the liquid supernatant was dialyzed (MWCO 14000) against deionized water for 3 d with repeated change of water. Finally, the solution of P(Py-TA) NPs were obtained and stored at 4 °C for further use.

1.2 Transparency

The transmission spectra of the hydrogel were measured on a UV-visible spectrometer equipped with a deuterium lamp and tungsten lamps from 400 to 800 nm. The value of transmittance at 660nm is used as the index of the transparency of hydrogel patches.

1.3 Swelling characterization

In order to evaluate the water uptake capacity of the hydrogels, the swelling behaviors of three kinds of hydrogels, including PAM, P(AM-Aa), and P(Py-TA)/CHA were tested. The weight of the initial hydrogel was recorded as W_0. Then, the hydrogels were soaked in deionized water for 7 days. At different time intervals, the weight of the hydrogels was recorded, denoted as W_s. Three parallel samples were used for the tests. The water uptake was calculated using the following Eq (1):

$$\text{Water uptake (W\%)} = (W_S - W_0)/W_0 \times 100\% \quad (1)$$

1.4 Rheological tests

Rheological tests of the hydrogels were using a rheometer (TA Discovery, DHR) fitted with 25 mm diameter parallel plate geometry. The storage modulus (G′), loss modulus (G″), and tan (delta) (tan δ) were monitored.

1.5 Mechanical property measurement

The mechanical properties of hydrogels were tested on a universal testing machine (Instron 5944) with a 100 N load cell. For tensile tests, the hydrogel was made into dumbbell shapes with a length of 40 mm, a gauge length of 12 mm, a width of 5 mm, and a thickness of 1 mm. The stretch rate was fixed at 50 mm min^{-1} for the normal tensile tests. The stress (σ) was determined as the loading force divided by the original specimen cross-sectional area, and the strain (ε) was defined as the deformed length divided by the original length of the samples. The elastic modulus (E) was calculated according to the initial linear slope of the stress−strain curve. The toughness was assessed by the extension work at fracture (W), which was obtained by integrating the area underneath the stress−strain curve. The strength and ductility product are a comprehensive performance indicator to characterize levels of strength and toughness at a static state. It is the product of the tensile strength and the maximum elongation, showing the absorbed energy of materials during tensile test.

The strength and ductility product (MPa %) = Maximum tensile strength (MPa) × Maximum tensile strain (%)

1.6 Adhesion ability tests

The universal testing machine (Instron 5944) was used to evaluate the adhesive capacity of the hydrogel with different substrates. The contact area of the hydrogel to different materials was 20

mm × 20 mm, after being pressed by 50 g weight for 5 min, the tensile lap shear was tested immediately, the shear adhesive strength was calculated as the maximum load divided by the contact lap area. All the experiments were performed in triplicate to reduce the error.

1.7 Electrical property tests

The electrochemical properties of hydrogel patch were recorded using a electrochemical workstation (CHI660C) by a two-probe method. The hydrogel was sandwiched between two pieces of copper for the measurement. During the impedance measurement, the voltage was kept constant at 50 mV and the frequency range is 10^6 to 10^{-1} Hz. The electrical conductivity of the hydrogel was calculated according to the following Eq (2).

$$\sigma = L/(R \times A) \quad (2)$$

where, L is the distance between the two pieces of copper; R is the value of the impedance obtained; A is the contact area between the hydrogel and the copper sheets.

Gauge factor (GF) was an important index for evaluating the sensitivity of hydrogel sensors.

$$GF = [(R - R_0)/R_0]/\varepsilon \quad (3)$$

Where, R_0 is the initial resistance of the hydrogel before stretching; R is the real-time resistance of the hydrogel after stretching; ε is applied strain.

1.8 Biocompatibility study

Biocompatibility studies have been carried out as in our previous studies.[1] Fibroblasts, L929 cells, a cell in connective tissue that produces collagen and other fibers associated with wound repairing was chosen as model cell to evaluate the cytotoxicity of hydrogel by CCK-8 assays and Live/Dead staining. All the samples were sterilized under UV irradiation for 60 mins. L929 cells was cultured in hyclone supplemented with 10% Fetal Bovine Serum (FBS, Gibco), 100 U mL^{-1} penicillin and 100 μL mL^{-1} streptomycin. The L929 cells were seeded into 12-well culture plates

(Corning, USA) with a density of 1×10^5 cells/well and cultured overnight. After the hydrogel was put into culture plates and cultured for 1, 4, 7 days, the medium were removed and fresh medium with 10% CCK-8 solution (Beibo, China) was added into the wells, then incubated for 2 h at 37 °C in 5% CO_2. The absorbance values of resulting solutions were measured by a microplate reader (Multiskan EX, Thermo Fisher Scientific, Shanghai, China) at 450 nm. To evaluate the cell viability in the hydrogel, a live/dead assay (Biobe times Biotechnology, Changsha, China) was performed. On days 4 after cell seeding, the samples were incubated with 1 mM calcein-AM for 1 h and then incubated with 1 ug/mL propidium iodide (PI) for 5 min at 37°C. Next, the cell was imaged using fluorescence microscopy (Olympus IX71, Tokyo, Japan).

1.11 Blood clotting index (BCI) assay

To evaluate the hemostasis effect of different hydrogels, whole blood clotting test was investigated in vitro using untreated as the control, and P(AM-Aa), and P(Py-TA)/CHA hydrogels. The operating process was referred to the previous study, and the absorbance of each sample was measured using a microplate reader at 540 nm.[2] To evaluate the blood coagulation effect, the BCI is calculated by the following Eq (4):

$$BCI = A/B \times 100\% \quad (4)$$

In this formula, A represents the absorbance value of blood using each sample, and B represents the absorbance value of citrated blood (0.4 mL) in 30 mL of DI water at 540 nm.

1.12 In vivo blood coagulation study

In order to investigate the hemostatic performance of the P(Py-TA)/CHA hydrogel, hemorrhaging liver and tail hemorrhage rat model was incorporated into studies.[3] Briefly, rats were anesthetized by 10% chloral hydrate at the dose of 0.3 mL/100 g body weight by intraperitoneal injection and fixed on the worktop. The liver was exposed gently by an upper

abdominal incision and the extravasated peritoneal fluid was removed with gauze. The liver acupuncture bleeding model was prepared by a 15 G needle with the corkboard tilted at about 30°. The bleeding site was treated with the different samples immediately. Subsequently, the liver incision bleeding model and the tail cut bleeding model were prepared by scalpel and surgical scissors. The weight of filter paper was weighed in advance, and after the liver stops bleeding, the filter paper containing blood was weighed again evaluate the amount of bleeding, thus assessing blood coagulation effect of the P(Py-TA)/CHA hydrogel.

1.13 Diabetic rat model preparation and wound healing examination

All animal protocols were carried out according to National Institutes of Health's Guide for the Care and Use of Laboratory Animals (NIH Publications No.8023, revised 1978), and approved by the Animal Care and Use Committee of Jilin University. Adult male Sprague-Dawley rats aged 8-10 weeks were provided by Animal Center of Basic Medical College of Jilin University. The diabetic model was established by intraperitoneal injection of streptozotocin (STZ, Sigma-Aldrich, USA) at a dose of 65 mg kg^{-1}. After one week of STZ administration, the blood glucose level was detected through tail vein by an ONETOUCH® Ultra blood glucose meter (Johnson, UK). The blood glucose level more than 16.7 mmol L^{-1} is considered that the diabetic rat model was successfully prepared.

For diabetic wound healing detection, there were 30 rats were incorporated 3 weeks after hyperglycemia induced by STZ. Briefly, full-thickness skin defects with 10 mm diameter on the back of rats was prepared by the puncture biopsy instrument under anesthesia with 10% chloral hydrate. Then the wounds were administrated with different treatments, namely, untreated (abbreviated as Control group) and covered with P(Py-TA)/CHA hydrogel dressing (abbreviated as Hydrogel group). At the scheduled time points, the wound healing process was photographed

by a digital camera and quantitatively analyzed by Image J software. The residual wound area was calculated by the following formula: Residual wound area (%) = $S_n/S_0 \times 100\%$ (S_0: initial wound area, S_n: wound area at different time points).

1.14 Histology and immunohistochemical staining

At different time points during the healing process, rats were sacrificed and the tissues surrounding the wounds were collected, followed by being fixed in 4% paraformaldehyde solution. Subsequently, the samples were embedded in paraffin and about 5 μm thickness sections were prepared. According to the manufacturer's instructions, skin sections were conducted to histological observation by Hematoxylin and Eosin (H&E) and Masson's trichrome (MT) staining, and immunohistochemical evaluation by anti-CD31 antibody (ARG52748, Arigo) and anti-K14 antibody (clone MiB-1; Dako).

2 Supporting Tables

Table S1 The compositions of various hydrogels.

Code	AM (g)	MPBA (mg)	P(Py-TA) (mg)	Aa (mg)	MBA/AM (wt.%)	APS/AM (wt.%)	Water (mL)	P(Py-TA)/AM (wt.%)	Aa/AM (wt.%)
PAM	1.8	200	0	0	0.1	3.4	3	0	0
P(AM-Aa)	1.8	200	0	135	0.1	3.4	3	0	7.5
P(Py-TA)/CHA	1.8	200	36	0	0.1	3.4	3	2	0
P(Py-TA)/CHA	1.8	200	36	45	0.1	3.4	3	2	2.5
P(Py-TA)/CHA	1.8	200	36	90	0.1	3.4	3	2	5
P(Py-TA)/CHA	1.8	200	36	135	0.1	3.4	3	2	7.5
P(Py-TA)/CHA	1.8	200	18	135	0.1	3.4	3	1	7.5
P(Py-TA)/CHA	1.8	200	36	135	0.1	3.4	3	2	7.5
P(Py-TA)/CHA	1.8	200	54	135	0.1	3.4	3	3	7.5
P(Py-TA)/CHA	1.8	200	72	135	0.1	3.4	3	4	7.5

Table S2 Comparison of the main parameters of different types of conduction hydrogels in this work and previous works.

Conduction Type	Transparency	Maximum Strain	Refs.
Electronic	93.6%	1650	This work
Electronic	50%	510	[4]
Electronic	62%	100	[5]
Electronic	76%	20	[6]
Ionic	92%	500	[7]
Electronic	76%	2000	[8]
Ionic	95%	1100	[9]
Ionic	92%	1800	[10]
Ionic	91%	2000	[11]
Ionic	87%	650	[12]
Ionic	65%	1330	[13]
Ionic	81%	1680	[14]
Ionic	89%	630	[15]
Electronic	94.2%	522	[16]
Ionic	90%	350	[17]
Ionic	60%	350	[18]
Electronic	70%	100	[19]
Ionic	93%	510	[20]
Ionic	89%	1200	[21]
Ionic	85.4%	2100	[22]

Table S3 The results of the glucose levels at DFUs of mice obtained from P(Py-TA)/CHA hydrogels and commercial glucometer.

Code	P(Py-TA)/CHA Hydrogel (mM)	Commercial Glucometer (mM)
Mouse-1	23.6 ± 3.2	22.3 ± 1.3
Mouse-2	21.4 ± 5.1	23.6 ± 2.4
Mouse-3	24.3 ± 4.4	25.8 ± 1.6

3 Supporting Figures

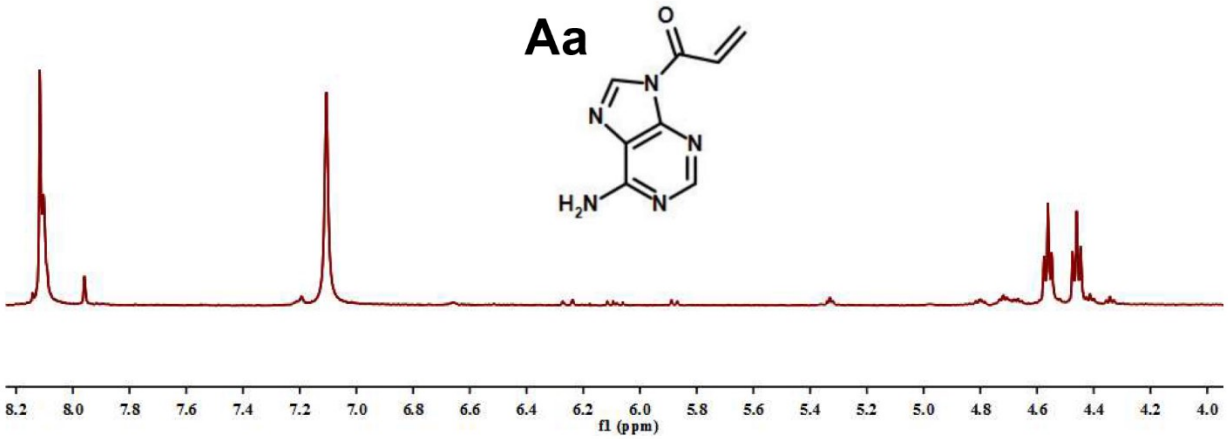

Fig. S1 ^{1}H NMR spectrum of Aa in D_2O.

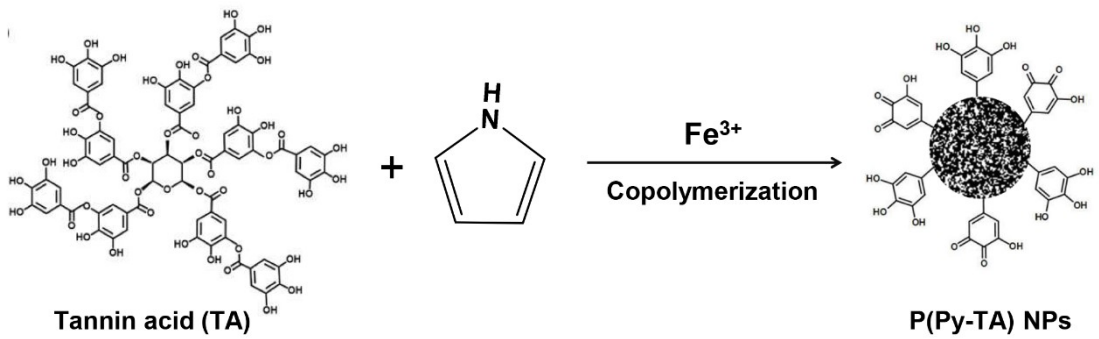

Fig. S2 Diagram of the formation of hydrophilic P(Py-TA) NPs.

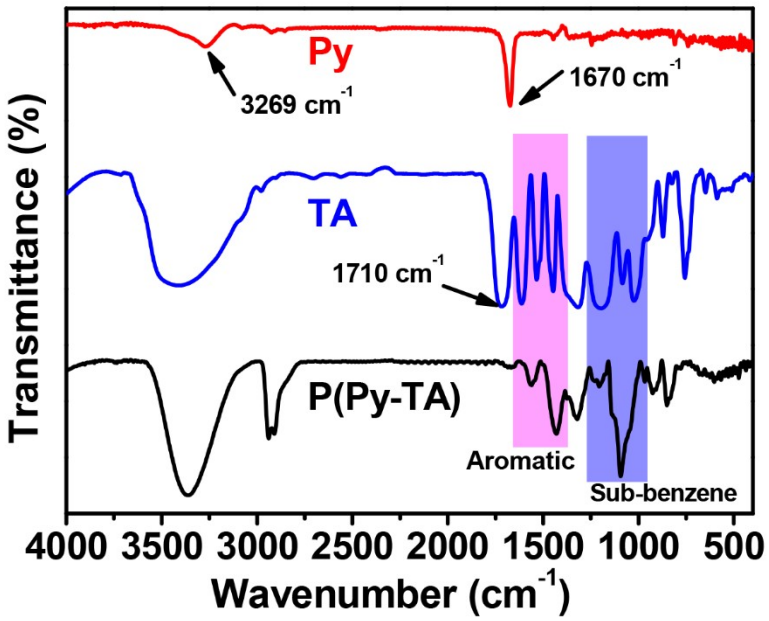

Fig. S3 FTIR spectrum of Py, TA and P(Py-TA) NPs. The characteristic vibration peaks at 1710 cm^{-1} correspond to C=O groups. The other characteristic peaks at 1612, 1533, and 1442 cm^{-1} can be assigned to aromatic compound stretching, and the characteristic peaks at 1195, 1083, and 1024 cm^{-1} refer to the vibration of substituted benzene rings.

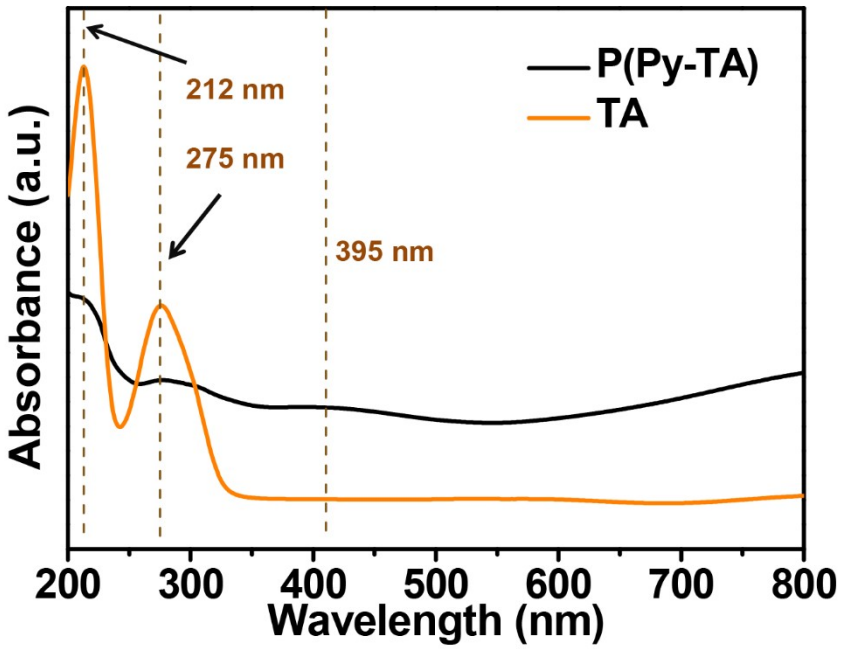

Fig. S4 UV−vis absorption spectra of TA and P(Py-TA) NPs solutions.

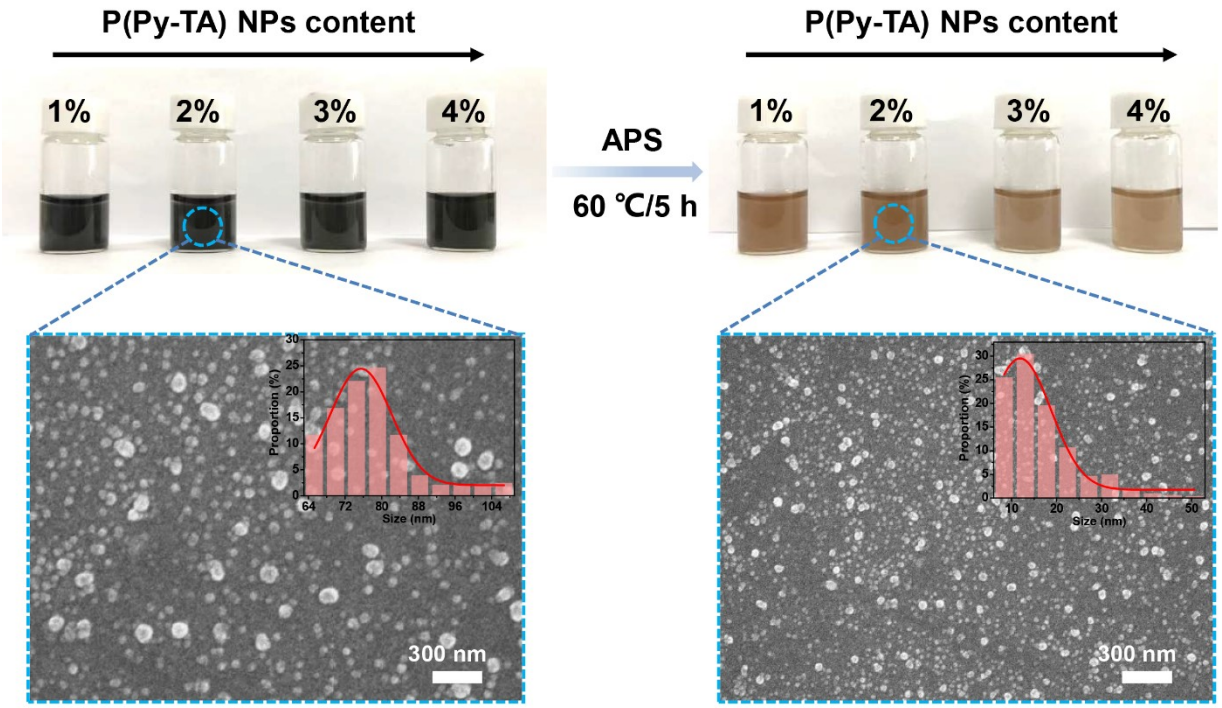

Fig. S5 The degradation of different contens of P(Py-TA) NPs dispersion (1%-4%), and the relevant SEM images and DLS analysis results (the inset diagrams) of 2% P(Py-TA) NPs dispersion.

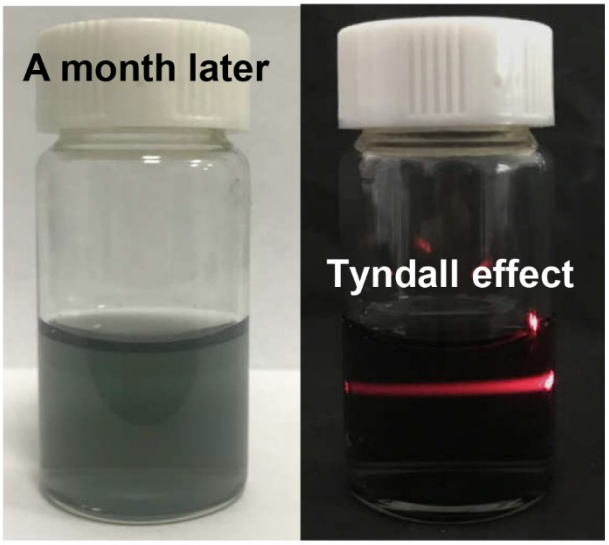

Fig. S6 The monodispersity of P(Py-TA) NPs after standing for a month, and the corresponding Tyndall effect by laser irradiation.

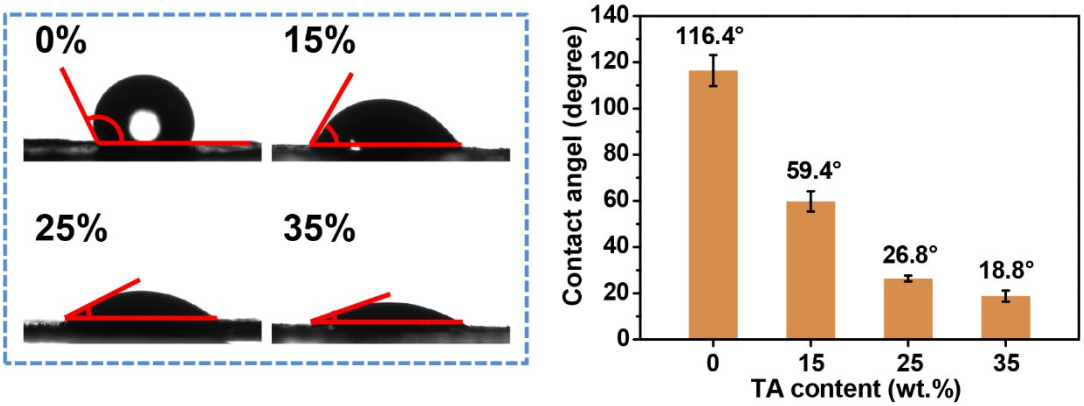

Fig. S7 Water contact angle of PPy and P(Py-TA) (with different TA content) coated film. Error bars represent standard deviation from the mean of 5 samples.

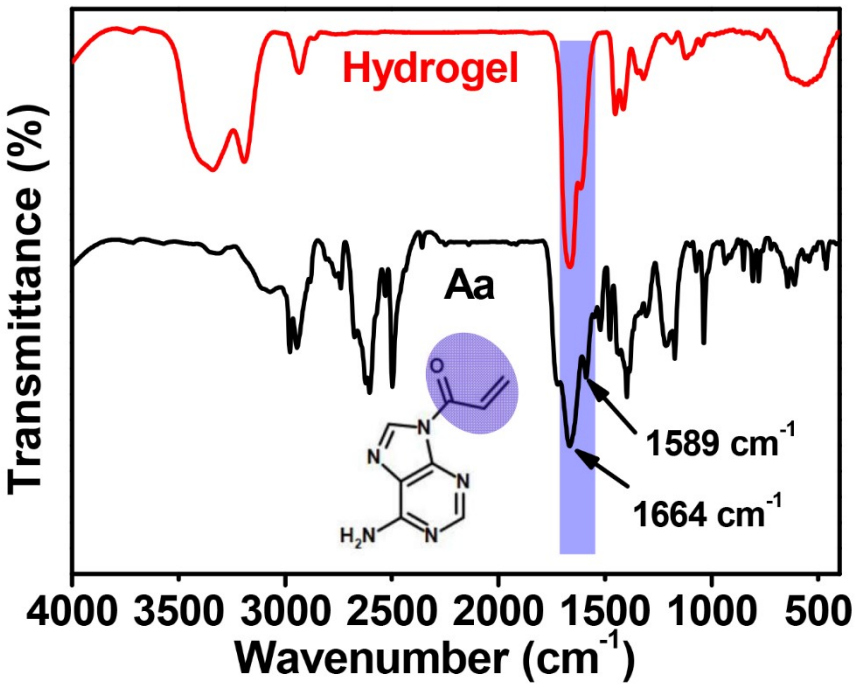

Fig. S8 FTIR spectrum of Aa and the P(Py-TA)/CHA hydrogel. The strong bands at 1589 cm^{-1} and 1664 cm^{-1} were associated with acrylic groups of Aa.

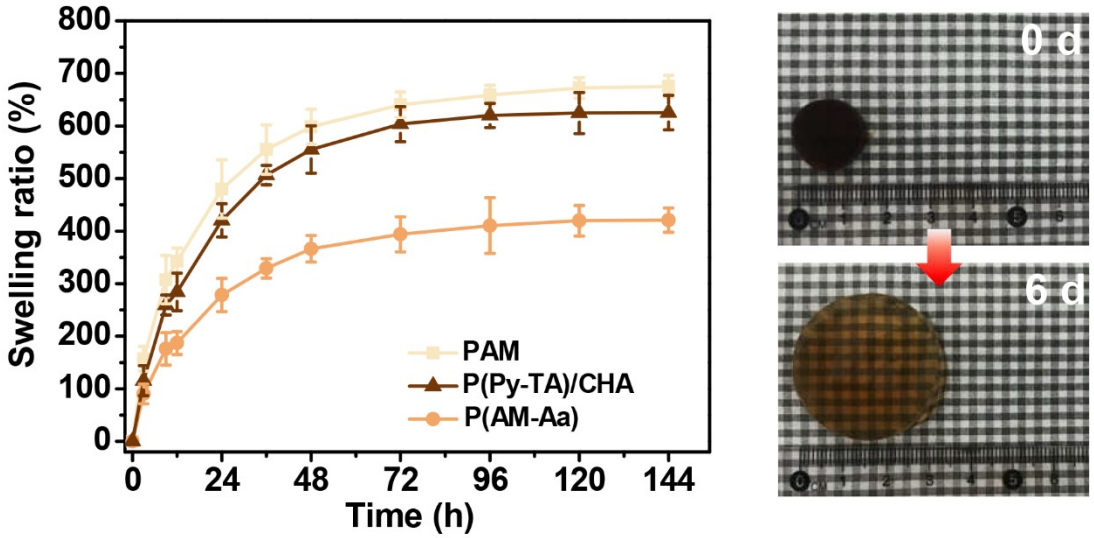

Fig. S9 The swelling kinetics of PAM, P(Py-TA)/CHA and P(AM-Aa) hydrogels incubated in distilled water for different times, respectively, and the digital images of P(Py-TA)/CHA hydrogel before and after swelling for 6 days.

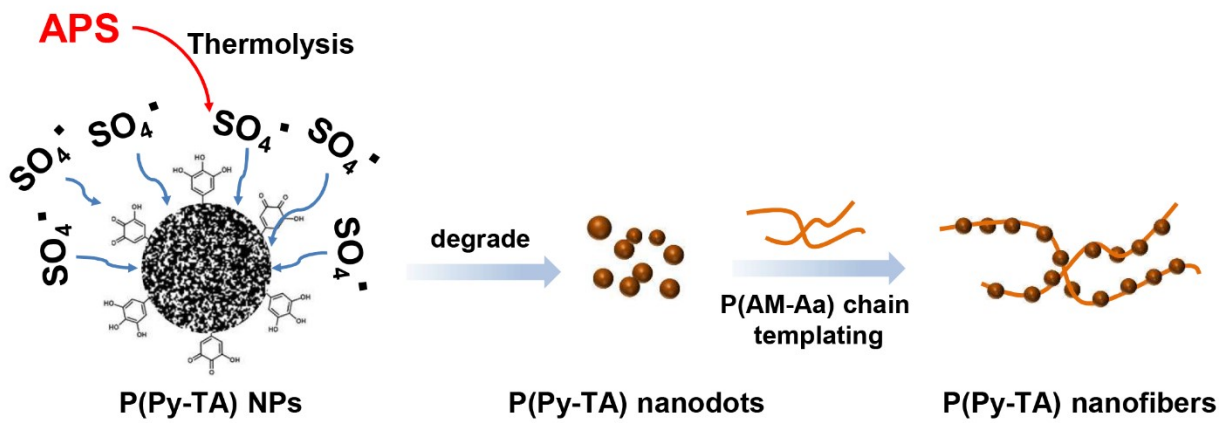

Fig. S10 In situ formation of P(Py-TA) nanofibrils. During the process, APS generated radicals that continuously degraded the P(Py-TA) NPs into nanodots, which self-assembled to form nanofibrils under the templating effect of the P(AM-Aa) chains.

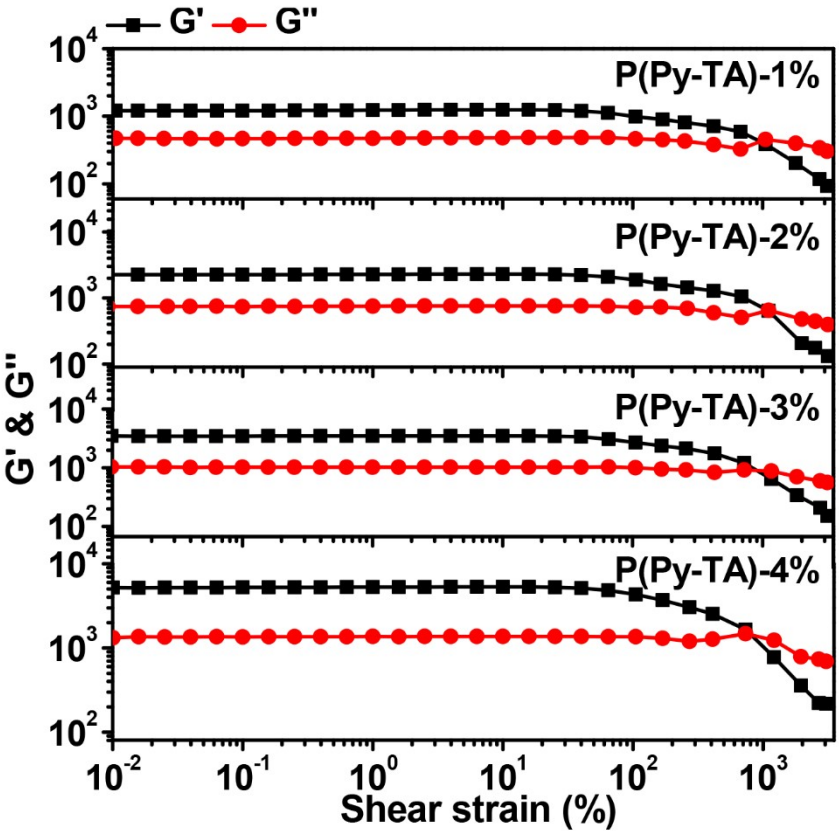

Fig. S11 The strain amplitude sweep of hydrogel patch with different P(Py-TA) NPs contents.

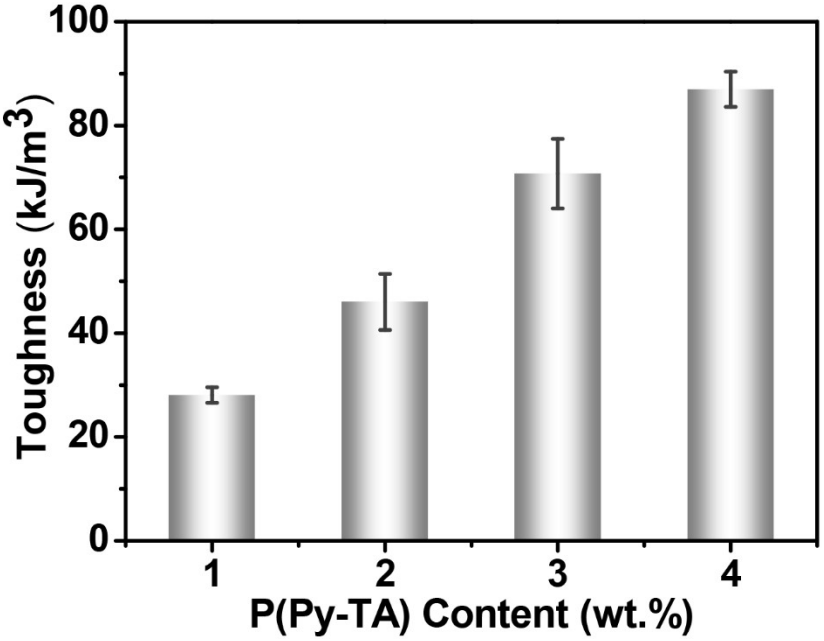

Fig. S12 The toughness of the hydrogel patch with different P(Py-TA) NPs contents.

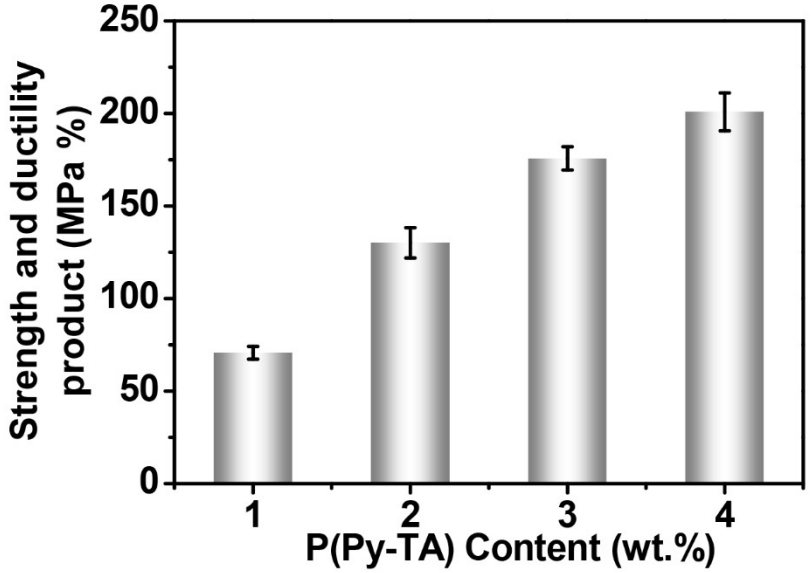

Fig. S13 The strength and ductility product of the hydrogel patch with different P(Py-TA) NPs contents.

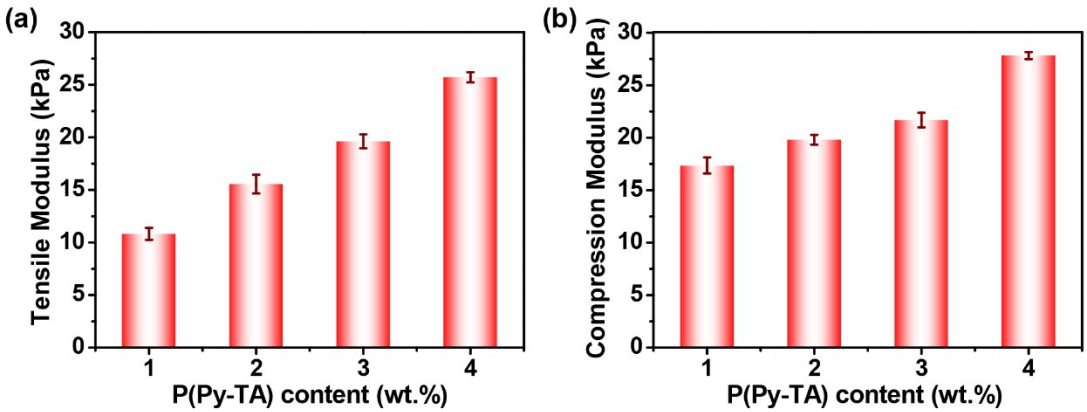

Fig. S14 The corresponding a) tensile modulus and b) compression modulus of the P(Py-TA)/CHA hydrogel patch at different P(Py-TA) NPs concents.

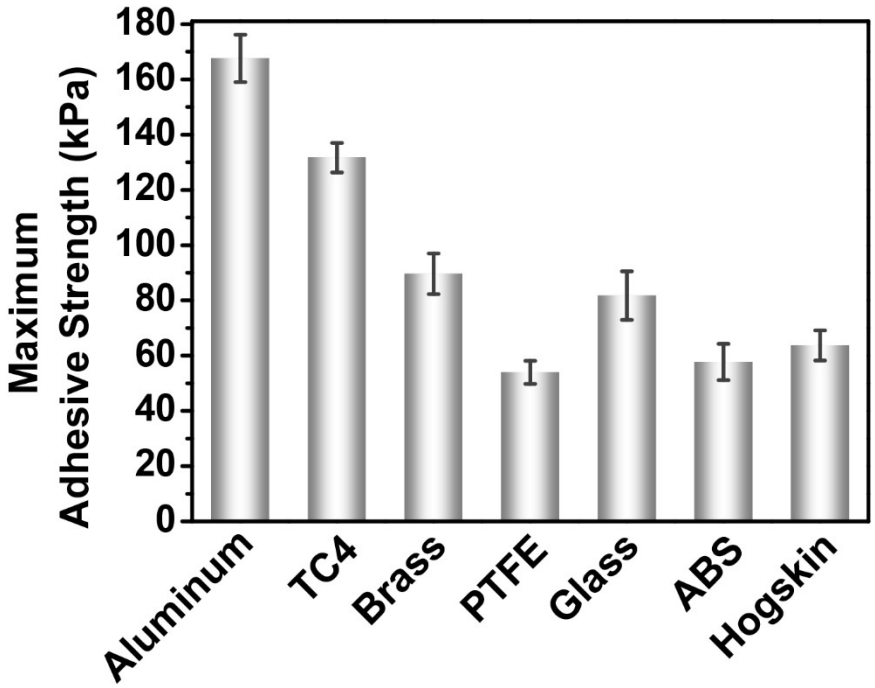

Fig. S15 The corresponding maximum adhesive strength of hydrogel patch on various substrate surfaces.

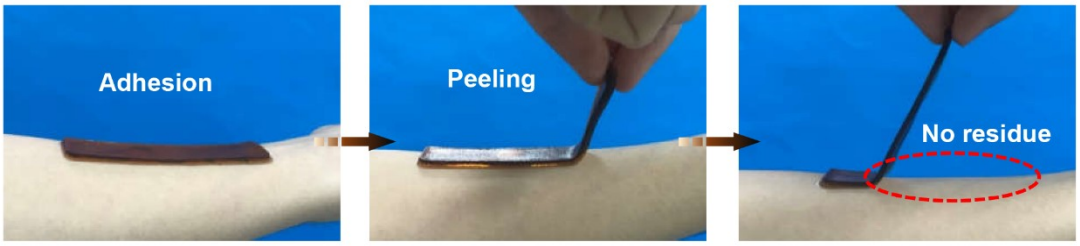

Fig. S16 The hydrogel pacth displayed good tissue adhesiveness on skin and no residue was observed after peeling.

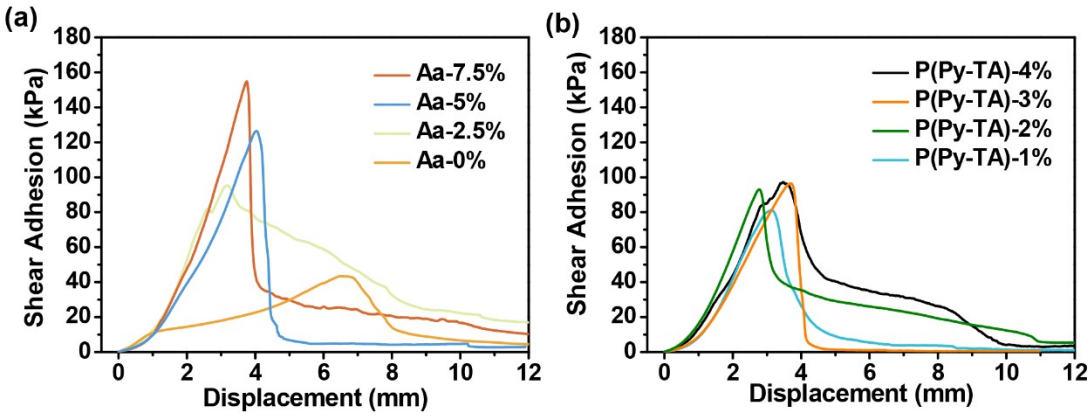

Fig. S17 Shear adhesion curves of the hydrogel patch with different a) Aa and b) P(Py-TA) NPs concentrations.

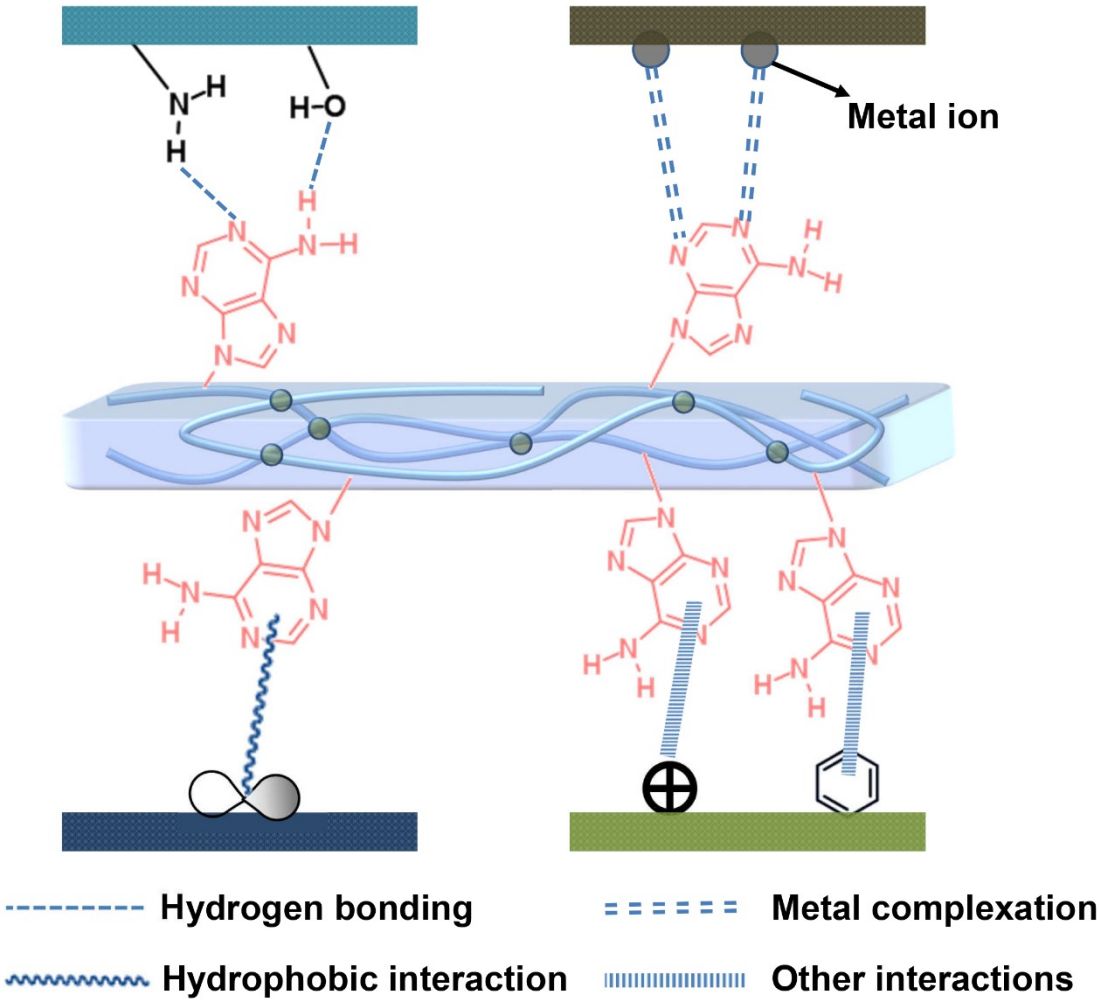

Fig. S18 Possible adhesion mechanisms including hydrogen bonding, metal complexation, hydrophobic interaction, and other interactions (cation–π and/or π–π stacking).

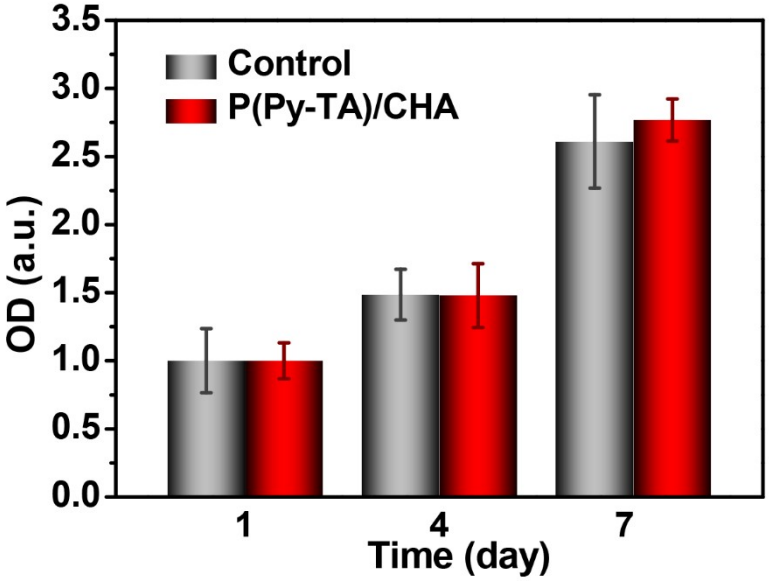

Fig. S19 Proliferation of L929 cells cultured for 1, 4 and 7 days (n = 3).

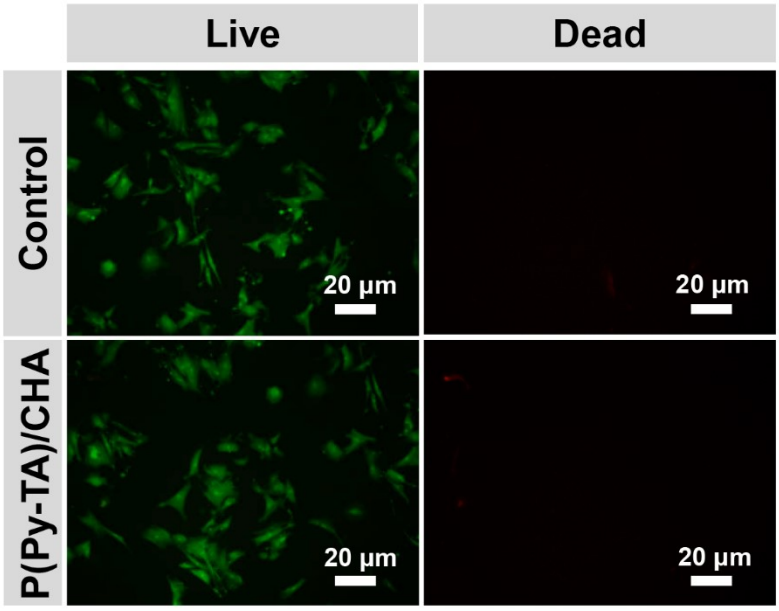

Fig. S20 Live/Dead staining of L929 cells for 3 days. Live cells appear green and dead cells appear red.

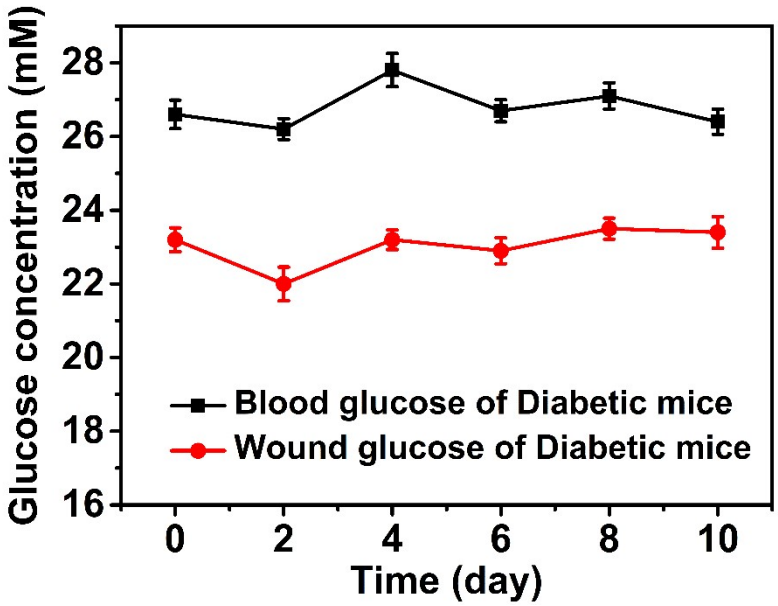

Fig. S21 Glucose concentrations in blood and wound exudate of diabetic mice from day 0 to day 10 after injury.

4. References

[1] H. Bai, Y. Zhao, C. Wang, Z. Wang, J. Wang, H. Liu, Y. Feng, Q. Lin, Z. Li, H. Liu, *Theranostics*, 2020, **10**, 4779–4794.

[2] X. Liu, Y. Niu, K. Chen, S. Chen, *Mater. Sci. Eng. C*, 2017, **71**, 289–297.

[3] E. Lih, J. Lee, K. M. Park, K. D. Park, *Acta Biomater.*, 2012, **8**, 3261–3269.

[4] G.-P. Hao, F. Hippauf, M. Oschatz, F. M. Wisser, A. Leifert, W. Nickel, N. *ACS Nano*, 2014, **8**, 7138–7146.

[5] E. Roh, B.-U. Hwang, D. Kim, B.-Y. Kim, N.-E. Lee, *ACS Nano*, 2015, **9**, 6252–6261.

[6] Ankit, N. Tiwari, M. Rajput, N. A. Chien, N. Mathews, *Small*, 2018, **14**, 1702312.

[7] G. Ge, Y. Zhang, J. Shao, W. Wang, W. Si, W. Huang, X. Dong, *Adv. Funct. Mater.*, 2018, **28**, 1802576.

[8] L. Han, L. Yan, M. Wang, K. Wang, L. Fang, J. Zhou, J. Fang, F. Ren, X. Lu, *Chem. Mater.*, 2018, **30**, 5561–5572.

[9] S. Zhang, Y. Zhang, B. Li, P. Zhang, L. Kan, G. Wang, H. Wei, X. Zhang, N. Ma, *ACS Appl. Mater. Interfaces*, 2019, **11**, 32441–32448.

[10] Y. Gao, F. Jia, G. Gao, *Chem. Eng. J.*, 2019, **375**, 121915

[11] Z. Jia, Y. Zeng, P. Tang, D. Gan, W. Xing, Y. Hou, K. Wang, C. Xie, X. Lu, *Chem. Mater.*, 2019, **31**, 5625–5632.

[12] Y. Ye, Y. Zhang, Y. Chen, X. Han, F. Jiang, *Adv. Funct. Mater.*, 2020, **30**, 2003430.

[13] J. Wu, Z. Wu, W. Huang, X. Yang, Y. Liang, K. Tao, B.-R. Yang, W. Shi, X. Xie, *ACS Appl. Mater. Interfaces*, 2020, **12**, 52070–52081.

[14] Q. Wang, X. Pan, C. Lin, X. Ma, S. Cao, Y. Ni, *Chem. Eng. J.*, 2020, **396**, 125341.

[15] J. Yu, C. Dang, H. Liu, M. Wang, X. Feng, C. Zhang, J. Kang, H. Qi, *Macromol. Mater. Eng.*, 2020, **305**, 2000475.

[16] X. Chen, M. He, X. Zhang, T. Lu, W. Hao, Y. Zhao, Y. Liu, *Macromol. Chem. Phys.*, 2020, **221**, 2000054.

[17] C. Zhang, Y. Zhou, H. Han, H. Zheng, W. Xu, Z. Wang, *ACS Nano*, 2021, **15**, 1785–1794.

[18] J. Wen, J. Tang, H. Ning, N. Hu, Y. Zhu, Y. Gong, C. Xu, Q. Zhao, X. Jiang, X. Hu, L. Lei, D. Wu, T. Huang, *Adv. Funct. Mater.*, 2021, **31**, 2011176.

[19] E. P. Gilshteyn, S. Lin, V. A. Kondrashov, D. S. Kopylova, A. P. Tsapenko, A. S. Anisimov, A. J. Hart, X. Zhao, A. G. Nasibulin, *ACS Appl. Mater. Interfaces*, 2018, **10**, 28069–28075.

[20] J. Mao, C. Zhao, L. Liu, Y. Li, D. Xiang, Y. Wu, H. Li, *Compos. Commun.*, 2021, **25**, 100733.

[21] J. Yu, M. Wang, C. Dang, C. Zhang, X. Feng, G. Chen, Z. Huang, H. Qi, H. Liu, J. Kang, *J. Mater. Chem. C*, 2021, **9**, 3635–3641.

[22] C. Sun, C. Hou, H. Zhang, Y. Li, Q. Zhang, H. Wang, *APL Materials*, 2021, **9**, 011101.